# Cyclophosphamide Enhances Cancer Antibody Immunotherapy in the Resistant Bone Marrow Niche by Modulating Macrophage FcγR Expression

Ali Roghanian[1,2,3*], Guangan Hu[1], Christopher Fraser[1], Maneesh Singh[1], Russell B. Foxall[2,3], Matthew J. Meyer[4], Emma Lees[4], Heather Huet[4], Martin J. Glennie[2,3], Stephen A. Beers[2,3], Sean H. Lim[2,3], Margaret Ashton-Key[2,3], Stephen M. Thirdborough[4], Mark S. Cragg[2,3], Jianzhu Chen[1*]

[1]Koch Institute for Integrative Cancer Research and Department of Biology, Massachusetts Institute of Technology, Cambridge, Massachusetts 02142, USA; [2]Antibody and Vaccine Group, Centre for Cancer Immunology, Cancer Sciences Unit, Faculty of Medicine, University of Southampton, Southampton, SO16 6YD, UK; [3]Cancer Research UK Centre, University of Southampton, Southampton, SO16 6YD, UK.; [4]Novartis Institute for Biomedical Research, Inc., 250 Massachusetts Avenue, Cambridge, MA 02139, USA;

*** Corresponding authors**: Ali Roghanian at A.Roghanian@soton.ac.uk or aroghani@mit.edu and Jianzhu Chen at jchen@mit.edu

**Running title:** Cyclophosphamide activates BM macrophage effector functions

**Keywords:** Cyclophosphamide, monoclonal antibody, macrophage, Fcγ receptors, bone marrow, resistant microenvironment, cancer

**Conflicts of Interest:** The authors declare no potential conflicts of interest.

**Abstract**

Therapy-resistant microenvironments represent a major barrier toward effective elimination of disseminated cancer. Many hematologic and solid tumors are resistant to therapeutic antibodies in the bone marrow (BM), but not in the periphery (*e.g.*, spleen). We recently showed that cyclophosphamide (CTX) sensitizes the BM niche to antibody therapeutics. Here we show that (i) the BM resistance is partly induced by tumor and partly due to the intrinsic BM microenvironment; (ii) CTX treatment overcomes both resistance mechanisms by activating macrophage migration and phagocytosis, including significant upregulation of activatory Fcγ receptors (FcγRIII and FcγRIV) and downregulation of the inhibitory FcγRIIB; and (iii) CTX also synergizes with cetuximab (anti-EGFR) and trastuzumab (anti-Her2) in eliminating metastatic breast cancer in the BM of humanized mice. These findings provide new insights into the mechanisms by which CTX synergizes with antibody therapies in niche-specific resistant organs and its applicability in treating BM-resident tumors.

**Significance**

- Compared to those in the spleen, macrophages in the BM express a significantly higher level of the inhibitory FcγRIIB and lower levels of activatory FcγRIII and FcγRIV.
- Tumor induces BM resistance to antibody therapy by upregulating the inhibitory FcγRIIB and downregulating activatory FcγRIII and FcγRIV expression on macrophages in both humans and mice.
- CTX overcomes both the intrinsic and tumor-induced resistance to antibody immunotherapy in the BM by upregulating the activatory FcγRIII and FcγRIV and downregulating the inhibitory FcγRIIB expression on macrophages.
- Transcriptome analysis suggests that CTX activates IFN-γ and TNF-α signaling in human and mouse BM macrophages *in vivo*.

## Introduction

Monoclonal antibody (mAb) is a major modality for cancer treatment because of its target-specificity, efficacy and low toxicity. Accumulating evidence suggests that mAb therapeutics can efficiently eliminate leukemia and lymphomas in the peripheral organs, such as spleen, but their efficacy is much lower in the bone marrow (BM) (*1, 2*). Similarly, metastasis of solid tumors, such as breast cancer, into the BM is often associated with poor treatment outcome and patient survival. These findings suggest that BM is a highly resistant organ to antibody-mediated elimination of tumor cells (*3*). Overcoming the BM resistance in cancer antibody immunotherapy is of significant clinical importance.

Therapeutic efficacy of mAb often relies on immune effector cells, including macrophages and natural killer (NK) cells (*4-7*). Binding of mAb to its target on malignant cells flags them for destruction by effector cells through FcγR-mediated antibody-dependent cellular cytotoxicity (ADCC) and phagocytosis (ADCP) (*8*). ADCC induces apoptosis/lysis of target cells by degranulation of effector cells such as NK cells. ADCP refers to the engulfment and digestion of mAb-opsonized targets by macrophages. Humans express up to six FcγRs (FcγRI [CD64], FcγRIIA [CD32A], FcγRIIB [CD32B], FcγRIIC [CD32C], FcγRIIIA [CD16A] and FcγRIIIB [CD16B]), with only FcγRIIB being a classical inhibitory immunoglobulin G (IgG) receptor. In mice, there are three activatory FcγRs (FcγRI [CD64], FcγRIII [CD16], and FcγRIV [CD16-2]) and one inhibitory FcγR (FcγRIIB [CD32B]) (*5, 8, 9*). Engagement of the activatory FcγRs with the Fc portion of IgG results in cellular activation through immunoreceptor tyrosine-based activation motifs (ITAM). In contrast, the intracellular domains of inhibitory FcγRIIB contains immunoreceptor tyrosine-based inhibitory motifs (ITIM) and its ligation leads to inhibition of the effector cells (*9, 10*). Macrophages and NK cells express a number of activatory and/or inhibitory FcγRs depending on their tissue localization and microenvironmental cues (*9, 10*). We and others have shown that FcγR expression profiles on NK cells and macrophages are critical for therapeutic efficacy of mAb; with almost all therapeutic mAb

relying on appropriate FcγR engagement for optimal activity (*4, 6, 11, 12*). Modulation of the FcγR expression profile and the activatory to inhibitory (A:I) FcγR ratio can alter mAb efficacy (*9, 13-15*). Low A:I FcγR ratio, due to a reduction in activatory FcγRs and/or elevation of inhibitory FcγRIIB, is a common feature of the immunosuppressive tumor microenvironment (*13*). In particular, expression of the inhibitory FcγRIIB, which is known to suppress anti-cancer mAb immunotherapy (*10, 16*), is significantly increased on macrophages residing in the tumor microenvironment (*13, 14, 17*).

Cyclophosphamide (CTX) is an alkylating agent with potent effects on various components of the immune system and can synergize with mAb therapeutics (*1, 18-22*). Low-dose CTX therapy is able to transiently deplete suppressive regulatory T cells (Tregs) in both preclinical models and in patients, leading to clinical benefit (*20, 22-24*). This is because, compared to effector T cells, Tregs have metabolic adaptations that make them more susceptible to CTX-mediated cytotoxicity (*25*). We and others have shown that CTX treatment leads to recruitment and activation of myeloid effector cells, including macrophages, into the BM of tumor-bearing mice (*1, 21, 26*). As a result, CTX overcomes BM resistant microenvironment and greatly enhances the efficacy of mAb therapeutics in eliminating human 'double-hit' lymphoma in the BM (*1*). CTX and other chemotherapies are also known to combine effectively with rituximab (anti-CD20) (*e.g.,* R-CHOP [rituximab plus CTX, doxorubicin, vincristine, and prednisone], R-CVP, etc.) for treating B cell malignancies in human (*27-30*). In agreement with the preclinical data, a high level of macrophages in the tumor has been shown to be associated with a favorable prognosis in follicular lymphoma (FL) patients undergoing R-CHOP, but not CHOP therapy (*31*). Despite these promising (pre)clinical effects, the underlying mechanisms by which CTX regulates macrophage function in different anatomical niches, such as the permissive lymphatic system organs and the resistant BM, is not fully understood.

The BM resistance niche is not unique to tumor-bearing mice (*1*); and BM resistance to mAb-mediated cell depletion has also been observed in immunocompetent wild-type mice and 'healthy' humanized mice (*2*). These observations highlight the existence of underlying intrinsic mechanisms

specific to the BM (*i.e.*, in steady state) and independent of tumor presence. Using immunodeficient NOD-SCID IL-2R$\gamma^{-/-}$ (NSG) and NSG mice reconstituted with the human immune system (*32*), which allow detailed analysis of both mouse and human macrophages in a niche-specific manner, we investigated the mechanisms by which CTX overcomes BM resistance. Our results reveal two mechanisms of BM resistance: one is intrinsic to the BM and the other is induced by resident tumor cells. CTX can overcome both resistance mechanisms by enhancing macrophage phagocytosis via downregulation of the inhibitory and upregulation of activatory FcγRs, respectively, and therefore synergizing with therapeutic mAb in eliminating target cells in the BM. We further show that the synergy extends to other direct targeting therapeutic antibodies and solid tumors that often metastasize into the BM. Our findings shed new light on the mechanisms and generality of CTX in overcoming BM resistance to antibody-mediated cancer immunotherapy.

## Materials and Methods

### Ethics Statement

All research with human samples and mice was performed in compliance with institutional guidelines, the World Medical Association's Declaration of Helsinki and the US Department of Health and Human Services Guide for the Care and use of Laboratory Animals. The MIT committee on the use of humans as experimental subjects (MIT COUHES) granted the research a waiver as all human samples (normally disposed of as medical waste) were collected anonymously with parental consent by a 3rd party and purchased from that party for the purposes of research. The MIT committee on animal care approved all the research components carried out *in vivo*. Animal experiments performed at the University of Southampton were approved by the local ethical committees and were performed under Home Office license P4D9C89EA. Ethical approval for the use of lymphoma patient tissues was granted under REC references 228/02/t (University of Southampton).

### Cell line establishment and cultures

Human $CD20^{+}$ lymphoma cell lines that also express GFP and luciferase were derived as follows. Briefly, human $CD34^{+}$ hematopoietic stem/progenitor cells (HSPCs) were transduced with a lentivirus expressing GFP and c-Myc and Bcl-2 oncogenes under the control of a B cell-specific Eμ enhancer/CD19 promoter (*33*). The transduced HSPCs were engrafted into NSG mice, where they rapidly gave rise to disseminated and aggressive human 'double-hit' lymphomas. The de novo generated lymphoma cells grew readily *in vitro* and were transduced with lentivirus expressing luciferase and puromycin resistance genes. Puromycin resistant lymphoma cells were derived and individual $GFP^{+}$ and human $CD20^{high}$ cells were sorted into a 96-well plate using a BD FACS Aria (Beckton Dickinson, NJ) and expanded *in vitro*. Individual clones were evaluated for bioluminescence using a 96-well plate reader. Established $GFP^{+}$ $CD20^{high}$ $luciferase^{+}$ lymphoma cells were cultured in RPMI 1640 containing 10% FCS, L-glutamine, 2-mercaptoethanol, non-essential

amino acids, sodium pyruvate, penicillin and streptomycin in an atmosphere of 5% $CO_2$ at 37°C. MDA-MA-231 cells were grown in glucose-rich DMEM medium supplemented with 10% FCS, l-glutamine, penicillin and streptomycin and incubated in an atmosphere of 5% $CO_2$ at 37°C.

**Hematopoietic stem/progenitor cells (HSPCs) isolation and generation of humanized mice**

Human fetal livers were obtained from aborted fetuses at 15–23 weeks of gestation, in accordance with the institutional ethical guidelines (Advanced Bioscience Resources, Inc., CA, USA). All women gave written informed consent for the donation of their fetal tissue for research. Fetuses were collected within 2 hours of the termination of pregnancy. Fetal liver tissue was initially cut into small pieces and digested with collagenase VI (2 mg/ml in Dulbecco's modified Eagle's medium [DMEM]) for 30 minutes at 37°C with periodic mixing. Single-cell suspensions were prepared by passing the digested tissue through a 100 μm cell strainer (BD Biosciences, NJ, USA). $CD34^+$ cells were purified with the use of a $CD34^+$ selection kit (Stem Cell Technologies, Vancouver, BC, Canada); the purity of $CD34^+$ cells was 90%–99%. Viable cells were counted by trypan blue exclusion of dead cells. All cells were isolated under sterile conditions.

NSG mice were purchased from the Jackson Laboratories (Bar Harbor, Maine, USA) and maintained under specific pathogen-free conditions in the animal facilities at MIT. To reconstitute mice, newborn pups (less than 2 days old) were irradiated with 100 cGy using a Gamma radiation source and injected intracardially with $CD34^+CD133^+$ cells (~$2 \times 10^5$ cells/recipient).

**Generation of humanized mice with metastasized breast cancer**

Adult humanized mice were injected with $5x10^5$ MDA-MA-231 human breast cancer cells carrying luciferase into the cardiac cavity (left ventricle) using a Vevo 770-ultrasound imaging system (VisualSonics) under general anesthesia, to model metastasis *in vivo*. Mice were treated ten days post

tumor cell engraftment. Tumor growth and spread was visualized using an IVIS Spectrum-bioluminescent imaging system.

**Tissue preparation, antibodies and flow cytometry**

At various time points following injection of NSG recipients with human HSPCs, mice were euthanized by $CO_2$ asphyxiation and blood, BM, spleen, lymph nodes and thymus were harvested. The spleens were digested by collagenase D (Sigma-Aldrich, USA) at 37°C for 30 min and the BM were flushed using syringes with a 27 gauge needle. All organs were then disrupted by grinding between frosted glass cover slips and single cell suspensions were prepared. Samples were lysed of red blood cells and cells were counted. FITC, PE, PerCP/cy5.5, APC, PE/Cy7 or APC/Cy7 conjugated antibodies, directed to human CD3, CD4, CD8, CD10, CD11c, CD14, CD15, CD16, CD19, CD20, CD33, CD34, CD41, CD45, CD56, HLA-DR, and mouse CD45.1, Ly6C, F4/80 were from Biolegend (USA). Human CD133 antibody was from Miltenyi Biotec (Germany). Fc-null specific mouse FcγR mAb ($F(ab')_2$ (FcγRI, clone AT152-9; FcγRIIB, clone AT130-2; FcγRIII, clone AT154-2; FcγRIV, clone 9E9) were produced following pepsin digestion (pH ~4.0) of monoclonal IgG at 37°C and subsequent HPLC purification and dialysis into PBS, as described (*34*); and labelled with FITC in-house, as previously reported (*35*). Cells were stained with appropriate combination of antibodies and then analyzed on LSR II flow cytometers (Beckton Dickinson, NJ, USA) in the MIT Koch Institute flow cytometry core facility. Cell sorting was performed on FACS Aria (Beckton Dickinson, NJ, USA) with a purity of 90%-99%; sorted cells were subjected to lysis and RNA was kept frozen at -80°C until further use. Dead cells were excluded from analysis by DAPI staining.

**Transcriptome analysis**

Splenic and BM mouse $hCD45^-$ $F4/80^+$ and human $hCD45^+$ $hCD14^+$ cells were sorted from naive and CTX-treated humanized mice on day 2 post intraperitoneal injection. Cells were lysed in RLT lysis

buffer containing β-mercaptoethanol and total RNA were extracted with RNeasy micro kit (Qiagen, USA) following the manufacturer's instruction. Total RNA was assessed for quality and quantified using a total RNA 6000 Nano LabChip on a 2100 Bioanalyzer (Agilent Inc., USA). cDNA libraries were prepared according to the Illumina TruSeq RNA Sample Preparation Guide for SMARTer Universal Low Input RNA Kit (Clontech, USA). Gene expression was measured using HiSeq 2000 system (Illumina, USA). RNAseq data from mouse and human macrophages were aligned to mm10 and hg19, respectively, using Bowtie2 v2.2.3 (*36*). The number of mapped reads were quantified by RSEM v1.2.15 (*37*). Differential expression analysis between paired samples before and after treatment was performed using edgeR (*38*) with $p$ <0.05 and >2 fold-change cut-offs. Differentially expressed genes were annotated using online functional enrichment analysis tool DAVID (http://david.ncifcrf.gov/) (*39*). Gene set enrichment analysis was performed using Broad Institute Software (*40*), with the gene list pre-ranked according to logFC values from the edgeR output. The M1 and M2 macrophage gene sets (*41*) were obtained from the Molecular Signature Database (http://software.broadinstitute.org/gsea/msigdb/). The heatmap figure was visualized with MeV (*42*). Human and Mouse orthologues were matched based on MGI database (http://www.informatics.jax.org/).

**Human lymphoma tissue immunohistochemistry (IHC)**

Formalin-fixed, paraffin-embedded (FFPE) sections (4 μm) of human lymphoma patients' lymph node (LN) and BM tissues were provided by Cellular Pathology, University Hospital Southampton NHS Foundation Trust. Sections were stained by immunohistochemistry (IHC) using the fully automated BOND-MAX IHC staining instrument (Leica Microsystems, Milton Keynes, UK), according to the manufacturer's instructions and as previously reported (*35*). Briefly, sections were deparaffinized, pre-treated for heat-induced antigen retrieval (BOND ER2 protocol), and incubated with hydrogen peroxide followed by rabbit anti-human FcγRIIB (clone EP888Y; Abcam, Cambridge, UK), at a 1 in 2000 dilution. The antibody was subsequently bound to the poly-HRP IgG reagent,

before incubation with 3,3'-diaminobenzidine (DAB). The sections were subsequently incubated with mouse anti-human CD68 (clone PG-M1; DAKO, Agilent Technologies LDA UK Limited, Stockport, UK) at a 1 in 250 dilution, which was then bound to the post primary IgG linker reagent. The substrate chromogen Fast Red was then applied. All sections were counterstained using hematoxylin and mounted in CV Ultra mounting media (Leica Microsystems, Milton Keynes, UK). All images taken at original magnification x400, using an Olympus BX51 microscope and UplanApo 40x/0.85 objective and x10 eyepiece objective with a Leica DFC425 camera and Leica LAS V4.12 software.

**Statistics**

Mann-Whitney and one-way ANOVA statistical tests were performed throughout using GraphPadPrism (version 7), as indicated. On bar graphs, where at least 3 experiments were performed, error bars represented standard deviation.

## Results

### CTX potentiates antibody immunotherapy of human lymphoma *in vivo*

In our study, we used a human $CD20^+$ B lymphoma cell line derived from overexpression of Myc and Bcl-2 (*33*) that also expressed the luciferase gene for easy *in vivo* monitoring of tumor burden by live mouse imaging. Lymphoma cells were engrafted into adult NSG mice by intravenous injection. Once tumor was established, mice were either not treated or treated with rituximab (anti-CD20; human IgG1), CTX, or rituximab plus CTX. Treatment of lymphoma-bearing mice with rituximab alone resulted in the depletion of lymphoma cells in the spleen, but not the BM (Figure 1A). CTX treatment alone did not significantly affect tumor burden. The combination treatment of rituximab and CTX resulted in almost complete tumor elimination, not only in the spleen, but also in the BM (Figure 1A and B). These data are consistent with our previous report using alemtuzumab (Supplemental Figure 1), a monoclonal antibody specific for human CD52 (*1*).

Therapeutic antibodies rely on the presence of innate immune effector cells, such as macrophages, via binding to their activatory FcγRs, in order to eliminate tumor cells *in vivo*. The observation that rituximab and alemtuzumab alone were only capable of depleting lymphoma cells from the spleen, but not BM, suggests that either there is not sufficient number of macrophages in the BM or BM-resident macrophages are less efficient in eliminating opsonized tumor cells than splenic macrophages. To test the latter possibility, we phenotyped the activatory and inhibitory FcγR expression on $F4/80^+$ macrophages in the spleen and BM of the same plain NSG mice (without tumor engraftment). Indeed, BM-resident $F4/80^+$ macrophages expressed higher levels of the inhibitory FcγRIIB and lower levels of activatory FcγRIII and FcγRIV (Figure 1C). This confirms that BM is a suppressive niche and BM-resident macrophages are likely less efficient in FcγR-mediated phagocytosis than those in the spleen.

To corroborate these findings, next we investigated whether human BM-resident macrophages also express higher levels of the inhibitory FcγRIIB in lymphoma patients. Diagnostic lymph node (LN) biopsies and staging BM trephines were obtained from four consented patients, one with diffuse large B cell lymphoma (DLBCL) and three with follicular lymphomas (FL). Paired LN and BM samples from each patient were mounted on the same slide and were double-stained with antibodies to human CD68 (macrophage marker) and FcγRIIB. Very few FcγRIIB$^{+}$ macrophages were found in LN sections, regardless of their proximity to lymphoma cells. FcγRIIB staining was weak, indicting a low level of expression (Figure 1D and Supplemental Figure 2). In contrast, the majority of CD68$^{+}$ macrophages in the BM stained strongly for FcγRIIB, indicating high levels of expression, both in areas with high lymphoma burden (left panel) and areas with no or low lymphoma burden (right panel) (Figure 1D and Supplemental Figure 2). As per our previous reports (*43*), FL cells and normal B cells expressed low to modest levels of FcγRIIB, which varied from patient to patient (Figure 1D). On the other hand, DLBCL cells expressed high levels of FcγRIIB, evident in both LN and BM (Supplemental Figure 2). These results show that the expression of FcγRIIB is considerably higher in macrophages in the BM than in the LN in lymphoma patients.

**CTX reprograms BM macrophages by increasing A:I FcγR ratio**

To investigate the effect of CTX on macrophage FcγR expression, we used plain NSG mice as they allow us to investigate the effect of CTX on macrophages in the absence of T, B, NK cells and importantly tumor cells. NSG mice were dosed with 100 mg/kg CTX and FcγR expression on F4/80$^{+}$ macrophages in the BM was analyzed 1, 2 and 3 days after treatment. Compared to untreated mice, the inhibitory FcγRIIB showed the greatest decrease on day 1 and day 2; whereas the activatory FcγRIII and FcγRIV showed the biggest increase on day 2 following CTX treatment (Figure 2A-B). We, therefore, focused on day 2 in subsequent experiments. Compared to FcγR expression on macrophages from BM of untreated mice, CTX treatment increased FcγRI by ~1.1-fold, FcγRIII by ~1.2-fold ($p< 0.0001$) and FcγRIV by ~1.45-fold ($p <0.001$) (Figure 2C). In contrast, CTX treatment

decreased FcγRIIB expression by ~1.4-fold ($p$ <0.0001). CTX treatment had no significant effect on the expression of FcγRs on macrophages in the spleen of the same mice (Figure 2D). Consistently, CTX significantly increased the A:I FcγR ratio on macrophages in the BM (Figure 2E), but not in the spleen (Figure 2F). Furthermore, CTX treatment increased expression of MHC class II and the costimulatory molecule CD86 on macrophages in the BM (Figure 2G), but not in the spleen. These observations demonstrate that CTX treatment reprograms macrophages to express higher levels of the activatory FcγRs and other immune-stimulatory factors, while reducing inhibitory FcγRIIB expression in a BM-specific manner.

**CTX activates BM macrophages in lymphoma-bearing mice *in vivo***

NSG mice were injected intravenously with human $CD20^+$ B lymphoma cells and 21 days later single cell suspensions were prepared from the BM and assayed for FcγR expression by myeloid cells. Compared to FcγR expression on BM macrophages in non-tumor-bearing NSG mice, BM macrophages in tumor-bearing mice expressed higher levels of FcγRIIB, but lower levels of FcγRIII and FcγRIV (Figure 3A-B). These results are consistent with previous observations of regulatory effects of tumor cells on FcγR expression (*9, 10, 13*).

The same as in non-tumor-bearing mice, treatment of tumor-bearing NSG mice with CTX for 2 days resulted in a higher expression of the activatory FcγRIII and FcγRIV, but a lower expression of the inhibitory FcγRIIB on BM macrophages (Figure 3C). Similarly, no significant change was observed in the FcγR expression by macrophages in the spleen of the treated tumor-bearing mice (Figure 3D). Consequently, the A:I FcγR ratio was significantly increased by more than two folds on BM macrophages (Figure 3E), but not on splenic macrophages in CTX-treated lymphoma-bearing mice versus untreated mice (Figure 3F). Notably this increase in A:I FcγR ratio on BM macrophages following CTX treatment was equivalent to that seen in the permissive spleen niche. Thus, CTX also enhances the A:I FcγR ratio on the BM-resident macrophages in tumor-bearing mice.

**CTX treatment potentiates antibody-mediated depletion of human B cells from the BM**

In addition to the resistant nature of BM in tumor-bearing mice (*1*), Nimmerjahn and colleagues also reported that the BM-resistance niche exists in tumor-free immunocompetent wild-type as well as 'healthy' humanized mice (*2*). To investigate whether CTX treatment potentiates depletion of normal human B cells, humanized mice were generated by engrafting human $CD34^+$ hematopoietic stem/progenitor cells (HSPCs) into NSG pups. Administration of rituximab alone in adult humanized mice resulted in efficient depletion of human $CD45^+CD19^+$ B cells from the circulation and spleen, but not BM (Figure 4 A-B), as reported previously (*2*). We then treated humanized mice with rituximab and CTX as single agents or in combination and measured the frequency of human B cells in the spleen and BM 7 days post treatment. Although CTX treatment resulted in a modest depletion of B cells from the spleen and the BM (Figure 4C-D), combination of rituximab and CTX resulted in a further significant depletion of B cells from both spleen and the BM. These results show that the poor depletion of B lymphoma cells from the BM by rituximab is not only due to the immunosuppressive tumor microenvironment, but also other intrinsic properties of the BM niche in general, which can be overcome by concomitant CTX treatment.

**CTX treatment potentiates antibody-mediated depletion of human breast cancer cells in the BM**

BM metastasis by breast, lung and liver cancers is often associated with treatment resistance. To investigate whether CTX synergizes with antibody therapeutics in eliminating BM metastasis of solid tumors, we generated metastatic human breast cancer-bearing mice by ultrasound-guided intracardiac injection of leuciferase-expressing MDA-MB-231 breast cancer cells into NSG mice or NSG mice reconstituted with human immune system. Although allogeneic human lymphoma cells were readily rejected in humanized mice, but not plain NSG mice following intravenous injection (Supplemental Figure 3A-B), breast cancer cells engrafted in unrelated humanized mice were not rejected, but grew slower as compared to those in NSG mice. When breast cancer cells were readily detected in the liver

and/or BM of NSG mice at around 10 days post engraftment, mice were either left untreated or treated with cetuximab, CTX or the combination of cetuximab and CTX once every 5 days. Tumor burden increased from day 10 to day 25 in untreated, cetuximab-treated and CTX-treated mice, as indicated by bioluminescence intensity (Figure 5A-B), although the increase of tumor burden was slower in CTX-treated mice. In contrast, tumor burden was stabilized from day 10 to 25 in mice treated with both CTX and cetuximab (Figure 5A-B). Consistently, BM was filled with tumor cells in untreated, cetuximab-treated and CTX-treated mice; whereas, BM was mostly cleared of tumor cells in CTX plus cetuximab-treated mice (Figure 5C-D). Untreated and cetuximab-treated mice exhibited earlier and bigger lesions of the bones; whereas CTX plus cetuximab-treated mice did not show any apparent bone lesion (Figure 5C-D). Survival of CTX plus cetuximab-treated mice was significantly longer than untreated and single agent-treated mice. Similarly, treatment with CTX plus trastuzumab also significantly extended the survival (Figure 5E).

In humanized mice engrafted with MDA-MB-231 breast cancer cells, CTX, but not cetuximab, treatment delayed the tumor progression; whereas tumor burden was significantly decreased following the combination therapy of CTX and cetuximab (Figure 5F-G). These results show that CTX synergizes with anti-EGFR therapeutics to eliminate breast cancer cells in the BM and liver, *i.e.*, working for different tumors and different therapeutic antibodies.

**CTX treatment reprograms human and mouse BM macrophages *in vivo***

To further investigate the broader immunomodulating effects of CTX *in vivo*, we performed transcriptional profiling of macrophages from the spleen and BM before and after CTX treatment. 'Healthy' humanized mice were treated with 100 mg/kg CTX for 2 days. Both human $CD45^+CD14^+$ and mouse $F4/80^+$ macrophages, from untreated control (naïve) and CTX-treated mice, were isolated by cell sorting from the BM and spleen of the same mice and used for RNA sequencing (RNAseq). Principal component analysis (PCA) of samples showed that both mouse and human macrophages

grouped according to the tissue of origins, independently of treatment (Figure 6A), suggesting that macrophage gene expression signatures are largely regulated by tissue microenvironment, as previously reported (*44, 45*). CTX induced significant changes in gene expression in the mouse macrophages: 247 genes were upregulated and 624 genes were downregulated in the spleen; and 346 genes were upregulated and 197 were downregulated in the BM. Among the significantly modulated genes, 59 were shared between the macrophages in the spleen and BM (Figure 6B). Functional pathway enrichment analysis revealed that most of the genes affected by CTX in the BM macrophages were involved in phagocytosis, antigen processing and presentation, apoptotic cell clearance, migration and immune defense (Figure 6C), all of which are hallmarks of an activated inflammatory phenotype involving TNF-α and IFN-γ signaling, as confirmed by gene set enrichment analysis (GSEA) (Figure 6D). In contrast, genes upregulated in splenic macrophages were mostly involved in transcription, cell proliferation, migration and immune/inflammatory response. Consistent with the flow cytometry immunophenotyping (Figure 2), in non-treated mice, the FcγRIIB transcript levels were higher in the BM macrophages than splenic macrophages, whereas the FcγRIII and FcγRIV transcript levels were lower in the BM macrophages than splenic macrophages (Figure 6E). Following CTX treatment, the levels of the FcγRIIB transcript were decreased whereas those of the FcγRIII and FcγRIV transcripts were increased in BM macrophages (Figure 6E). As a result, CTX treatment induced a significantly higher A:I FcγR ratio in BM-resident macrophages, but not the splenic macrophages. We also examined the expression of macrophage proinflammatory (M1) and anti-inflammatory (M2) genes by BM and splenic macrophages isolated from naïve non-treated mice (*41*). Splenic macrophages were significantly enriched for expression of 'M1-polarizing' genes; whereas BM-resident macrophages were enriched for expression of 'M2-polarizing' genes (Supplemental Figure 4A). CTX treatment induced a significant 'M2 to M1 shift' in the BM macrophages (Supplemental Figure 4B).

Similarly, CTX induced significant changes in gene expression in human macrophages *in vivo*: 37 genes were upregulated and 168 genes were downregulated in the spleen; and 61 genes were

upregulated and 47 genes were downregulated in the BM (Figure 6F). Among the significantly affected genes, 8 were shared between the two niches. Functional pathway enrichment analysis revealed that differentially expressed genes in the splenic macrophages were involved in transcription, DNA replication, immune responses and NF-κB; whereas those in the BM macrophages were involved in inflammatory/immune responses, chemotaxis and protein ubiquitination (Figure 6G). The same as mouse BM-resident macrophages, GSEA analysis revealed that TNF-α and IFN-γ signaling pathways were upregulated in BM-resident human macrophages (Figure 6H). We further compared genes shared between mouse and human macrophages from the spleen and BM of humanized mice. Several genes were similarly regulated by CTX treatment in both species, such as the upregulation of HSPB1 and SLC15A3 and downregulation of F13A1, PPM1L and PTDSS2 in splenic macrophages; and upregulation of SIGLEC1, SLC1A3, CDKN1A and CXCL10 and downregulation of ETS1, SEPT1, PGLYPR1 and ORM1 in BM-resident macrophages (Figure 6I).

**Discussions**

We have previously shown that alemtuzumab (anti-CD52) is effective in eliminating human B lymphoma in the peripheral organs, such as spleen and liver, but not the BM. The BM resistance can be overcome by combination chemoimmunotherapy of low-dose CTX and alemtuzumab, partly through recruitment of macrophages into the BM. In this study, we further investigated the nature of BM resistance, mechanism of action of CTX in overcoming the resistance and generality of CTX in synergizing with other therapeutic antibodies for effective elimination of solid tumors from the BM. We show that the BM resistance results partly from the intrinsic resistant property of the BM and partly from the tumor-induced suppressive microenvironment. In "healthy" humanized mice in the absence of tumor engraftment, administration of rituximab efficiently depleted human B cells from the peripheral blood and spleen, but not the BM, suggesting that the BM is a resistant niche in the absence of the tumor. The presence of tumor in the BM likely makes the BM even more resistant as indicated by the increased expression of the inhibitory FcγRIIB and decreased expression of activatory FcγRIII and FcγRIV by BM macrophages. Our findings are consistent with previous observations showing the intrinsic resistance of BM to antibody-mediated depletion of human B cells (*1, 2*) and induction of FcγRIIB expression on BM macrophages in the presence of tumor (*13, 17*). Consistent with the preclinical observations, we also demonstrate that in matched LN and BM samples from the same lymphoma patients, FcγRIIB is highly expressed by BM-resident $CD68^+$ macrophages, but not by macrophages in LN, regardless of their proximity to the tumor. In addition, our study extends the previous studies by showing that CTX chemotherapy can transiently overcome both the intrinsic resistant property of the BM and the resistance induced by tumor cells. We show that "healthy" human B cells are efficiently depleted by rituximab in humanized mice in the presence of CTX.

We further demonstrate that CTX overcomes the BM resistance in the presence or the absence of tumors through the same mechanisms. In the BM of both plain NSG mice (without tumor engraftment) and NSG mice with engrafted tumor, CTX activated BM-resident macrophages to increase the

expression of activatory FcγRIII and FcγRIV, but significantly decreased the expression of the inhibitory FcγRIIB at both the transcript and protein levels. No significant changes were observed in macrophage FcγR expression in the spleen, suggesting that CTX had less profound effects on these cells. As such, splenic macrophages are efficient at phagocytosing opsonized tumor cells *in vivo* (in the absence of CTX stimulation), implying their activation threshold is far lower than BM-resident macrophages. The organ-specific activation of macrophages is in agreement with our previous report, whereby a synergy was observed in tumor-bearing mice dosed with alemtuzumab and CTX within one day of each other (*1*). Interestingly, CTX treatment did not have the same influence on $Ly6C^+$ monocytes, and in fact resulted in an increased expression of the inhibitory FcγRIIB and overall lowering of the A:I FcγR ratio (data not shown), suggesting that CTX activation of myeloid cells is both organ- and myeloid cell subset (macrophage)-specific.

Moreover, we showed that CTX synergizes with antibody-mediated elimination of tumor cells in the BM could be extended to solid tumors, such as metastatic breast cancer, and other antibodies, such as cetuximab and trastuzumab. In both plain NSG mice and humanized mice with breast cancer engraftment, the combination treatment of CTX and cetuximab (or trastuzumab) efficiently eliminated tumor cells; whereas, CTX or cetuximab alone did not. A limited number of studies have investigated the clinical benefits of chemoimmunotherapy in treating metastatic breast cancer to date (*46, 47*); however, the full mechanism of action of such combination therapies is not yet clear. The observation that CTX is also capable of synergizing with cetuximab and trastuzumab to treat BM-metastasized human breast cancer cells in NSG and fully reconstituted humanized mice is of particular clinical importance. Firstly, it provides mechanistic insights in relevant *in vivo* models and emphasizes that CTX-induced activation of macrophages is independent of the cancer type in the resistant niche. Secondly, it highlights that CTX chemotherapy is able to potentiate the efficacy of different therapeutic antibodies, irrespective of the tumor origin and the target antigen. These encouraging results suggest that CTX may have a broader application in combination therapy with therapeutic antibodies and warrant further investigation. This combination therapy may also enhance the

therapeutic activity of certain immune checkpoint blocking antibodies, such as anti-CTLA-4, that have been suggested to exert their effect by preferentially depleting tumor-resident Tregs via ADCP (*48, 49*).

Our detailed transcriptional analysis of both mouse and human macrophages from CTX-treated humanized mice further shed light on the mechanism by which CTX activates macrophages in the BM. CTX treatment differentially activated both spleen- and BM-resident mouse and human macrophages. Gene signatures modulated in BM-resident macrophages represented immune- and inflammatory-related genes involved in phagocytosis, antigen processing and presentation, apoptotic cell clearance, migration and immune defense, consistent with increased activities. In agreement, GSEA analysis of murine and human macrophages suggested that IFN-γ and TNF-α signaling pathways were significantly induced by CTX treatment. Of note, and in contrast to splenic macrophages which had a 'M1-polarizing' gene signature, BM-resident macrophages were more enriched for 'M2-polarizing' genes in naïve non-treated mice, which significantly shifted towards 'M1' upon short-term CTX treatment. In addition to confirming a significantly higher A:I FcγR ratio in the mouse BM-resident macrophages, but not in splenic macrophages, at the transcriptome level, we identified several genes that were similarly affected by CTX in mouse and human macrophages from spleen and BM. The commonly upregulated genes identified in BM-resident macrophages included SIGLEC1 (CD169, sialoadhesin), HSPA1B (HSP70) and CXCL10. Both SIGLEC1 and HSPA1B are key factors implicated in macrophage phagocytosis. SIGLEC1, a member of the I-type lectin family, is induced by Toll-like receptor (TLR) agonists (TLR-7 and -9) and type I IFN (*50*). SIGLEC1 contributes to host defense via scavenging functions, strongly promoting macrophage activation and phagocytosis (*51*). HSPA1B encodes a 70-kDa heat shock protein and has been reported to activate macrophages and enhance phagocytosis (*52, 53*). Similarly, CXCL10 is an IFN-inducible chemokine, which is a chemotactic factor for T cells and myeloid cells (*54*). On the other hand, four genes (ETS1, SEPT1, PGLYPR1 and ORM1) were commonly downregulated in BM-resident mouse and human macrophages following CTX treatment. ETS1 is a transcription factor, induced by a variety of factors

including TNF-α, which is responsible for vascular inflammation and remodeling (*55*). Nevertheless, CTX did not reprogram BM macrophages into splenic macrophages as spleen and BM macrophages cluster separately, regardless of their activation status, consistent with strong effect of microenvironment on macrophage phenotype and activity (*44, 45*).

Our findings suggest modulating FcγRIIB as an attractive cancer immunotherapeutic target. In the case of cancer therapy, this was originally demonstrated by Clynes and colleagues, who showed that antibody therapy was significantly improved in FcγRIIB-deficient mice (*16*). Since this approach is not viable in the clinic, modulating FcγR expression and A:I FcγR ratio is an attractive way by which to augment antibody efficacy. FcγRIIB can be targeted by specific blocking antibody (*56, 57*) or its expression regulated by modulating the tumor microenvironment (*10, 13*). Our current data indicate that CTX treatment is able to selectively target BM-resident macrophages by lowering their inhibitory FcγRIIB and increasing their activatory FcγRs. This transient increase of A:I FcγR ratio on BM-resident macrophages, together with activation of macrophage for phagocytosis, migration, and apoptotic cell clearance could result in "superphagocytic" macrophages for eliminating antibody-bound tumor cells in the BM. These results are consistent and complementary to data from David Weinstock's group, where patient-derived xenograft models are used to study this phenomenon in 'double-hit' lymphoma therapy (personal communication).

In conclusion, our study further elucidates the nature of BM resistance, the mechanisms by which CTX synergizes with antibody therapeutics and generality of this synergy for other antibodies and human solid tumors. Despite major therapeutic advances, most hematological (*e.g.*, mature B cell malignancies) and metastatic solid cancers (*e.g.*, breast cancer) remain incurable (*58, 59*). One potential facet underpinning treatment resistance is the powerful pro-survival microenvironment in the BM (*28, 60-63*). Our current study adds to the growing evidence that CTX can be used to overcome

the suppressive BM microenvironment and therefore synergize with antibody-mediated elimination of tumor cells in the BM.

**Acknowledgements and Grant Support**

We would like to thank the Koch Institute Flow Cytometry (Glenn Paradis), Bioinformatics and Computing (Stuart Levin) and Animal Imaging and Preclinical Testing cores (Scott Malstrom) for their technical assistance, Starsha Kolodziej and Megan Kaiser for their support with generating and maintaining the humanized mice, Adam Drake for the parental lymphoma cell lines, Feng Shi for lentiviral vector expressing luciferase and puromycin, and Richard Hynes for MDA-MA-231 breast cancer cell line. We would also like to thank the Antibody and Vaccine Group antibody production team and Alison Tutt for the provision of FITC-labelled FcγR antibodies, Ruth French for advice on statistical analysis. This work was supported in part by a Bloodwise Visiting Fellowship grant (14043) to AR, the Southampton CRUK Experimental Cancer Medicine Centre, the Koch Institute Support (core) Grant P30-CA14051 from the National Cancer Institute, and NIH grants 1R01NS104315 and 1R35CA197605.

## References


1. C. P. Pallasch *et al.*, Sensitizing protective tumor microenvironments to antibody-mediated therapy. *Cell* **156**, 590-602 (2014).
2. A. Lux *et al.*, A humanized mouse identifies the bone marrow as a niche with low therapeutic IgG activity. *Cell reports* **7**, 236-248 (2014).
3. P. I. Croucher, M. M. McDonald, T. J. Martin, Bone metastasis: the importance of the neighbourhood. *Nat Rev Cancer* **16**, 373-386 (2016).
4. N. Gul *et al.*, Macrophages eliminate circulating tumor cells after monoclonal antibody therapy. *The Journal of clinical investigation* **124**, 812-823 (2014).
5. N. Gul, M. van Egmond, Antibody-Dependent Phagocytosis of Tumor Cells by Macrophages: A Potent Effector Mechanism of Monoclonal Antibody Therapy of Cancer. *Cancer research* **75**, 5008-5013 (2015).
6. S. A. Beers *et al.*, Antigenic modulation limits the efficacy of anti-CD20 antibodies: implications for antibody selection. *Blood* **115**, 5191-5201 (2010).
7. A. Mantovani, F. Marchesi, A. Malesci, L. Laghi, P. Allavena, Tumour-associated macrophages as treatment targets in oncology. *Nat Rev Clin Oncol* **14**, 399-416 (2017).
8. F. Nimmerjahn, S. Gordan, A. Lux, FcgammaR dependent mechanisms of cytotoxic, agonistic, and neutralizing antibody activities. *Trends in immunology* **36**, 325-336 (2015).
9. L. N. Dahal, A. Roghanian, S. A. Beers, M. S. Cragg, FcgammaR requirements leading to successful immunotherapy. *Immunological reviews* **268**, 104-122 (2015).
10. A. Roghanian, R. J. Stopforth, L. N. Dahal, M. S. Cragg, New revelations from an old receptor: Immunoregulatory functions of the inhibitory Fc gamma receptor, FcgammaRIIB (CD32B). *Journal of leukocyte biology*, (2018).
11. F. Nimmerjahn, J. V. Ravetch, Antibodies, Fc receptors and cancer. *Current opinion in immunology* **19**, 239-245 (2007).
12. R. Clynes, Antitumor antibodies in the treatment of cancer: Fc receptors link opsonic antibody with cellular immunity. *Hematology/oncology clinics of North America* **20**, 585-612 (2006).
13. L. N. Dahal *et al.*, STING Activation Reverses Lymphoma-Mediated Resistance to Antibody Immunotherapy. *Cancer research* **77**, 3619-3631 (2017).
14. S. Bournazos, T. T. Wang, J. V. Ravetch, The Role and Function of Fcgamma Receptors on Myeloid Cells. *Microbiology spectrum* **4**, (2016).
15. H. Benonisson *et al.*, High FcgammaR Expression on Intratumoral Macrophages Enhances Tumor-Targeting Antibody Therapy. *J Immunol* **201**, 3741-3749 (2018).
16. R. A. Clynes, T. L. Towers, L. G. Presta, J. V. Ravetch, Inhibitory Fc receptors modulate in vivo cytotoxicity against tumor targets. *Nature medicine* **6**, 443-446 (2000).
17. F. Arce Vargas *et al.*, Fc-Optimized Anti-CD25 Depletes Tumor-Infiltrating Regulatory T Cells and Synergizes with PD-1 Blockade to Eradicate Established Tumors. *Immunity* **46**, 577-586 (2017).
18. E. Proietti *et al.*, Importance of cyclophosphamide-induced bystander effect on T cells for a successful tumor eradication in response to adoptive immunotherapy in mice. *The Journal of clinical investigation* **101**, 429-441 (1998).
19. A. Sistigu *et al.*, Immunomodulatory effects of cyclophosphamide and implementations for vaccine design. *Seminars in immunopathology* **33**, 369-383 (2011).
20. M. Scurr *et al.*, Low-Dose Cyclophosphamide Induces Antitumor T-Cell Responses, which Associate with Survival in Metastatic Colorectal Cancer. *Clin Cancer Res* **23**, 6771-6780 (2017).
21. V. Radojcic *et al.*, Cyclophosphamide resets dendritic cell homeostasis and enhances antitumor immunity through effects that extend beyond regulatory T cell elimination. *Cancer immunology, immunotherapy : CII* **59**, 137-148 (2010).

22. F. Moschella *et al.*, Unraveling cancer chemoimmunotherapy mechanisms by gene and protein expression profiling of responses to cyclophosphamide. *Cancer research* **71**, 3528-3539 (2011).
23. M. Ahlmann, G. Hempel, The effect of cyclophosphamide on the immune system: implications for clinical cancer therapy. *Cancer Chemother Pharmacol* **78**, 661-671 (2016).
24. F. Ghiringhelli *et al.*, CD4+CD25+ regulatory T cells suppress tumor immunity but are sensitive to cyclophosphamide which allows immunotherapy of established tumors to be curative. *Eur J Immunol* **34**, 336-344 (2004).
25. M. T. Madondo, M. Quinn, M. Plebanski, Low dose cyclophosphamide: Mechanisms of T cell modulation. *Cancer Treat Rev* **42**, 3-9 (2016).
26. J. C. Doloff, D. J. Waxman, VEGF receptor inhibitors block the ability of metronomically dosed cyclophosphamide to activate innate immunity-induced tumor regression. *Cancer research* **72**, 1103-1115 (2012).
27. C. Nickenig *et al.*, Combined cyclophosphamide, vincristine, doxorubicin, and prednisone (CHOP) improves response rates but not survival and has lower hematologic toxicity compared with combined mitoxantrone, chlorambucil, and prednisone (MCP) in follicular and mantle cell lymphomas: results of a prospective randomized trial of the German Low-Grade Lymphoma Study Group. *Cancer* **107**, 1014-1022 (2006).
28. D. W. Scott, R. D. Gascoyne, The tumour microenvironment in B cell lymphomas. *Nat Rev Cancer* **14**, 517-534 (2014).
29. T. M. Habermann *et al.*, Rituximab-CHOP versus CHOP alone or with maintenance rituximab in older patients with diffuse large B-cell lymphoma. *Journal of clinical oncology : official journal of the American Society of Clinical Oncology* **24**, 3121-3127 (2006).
30. M. J. Keating *et al.*, Early results of a chemoimmunotherapy regimen of fludarabine, cyclophosphamide, and rituximab as initial therapy for chronic lymphocytic leukemia. *Journal of clinical oncology : official journal of the American Society of Clinical Oncology* **23**, 4079-4088 (2005).
31. M. Taskinen, M. L. Karjalainen-Lindsberg, H. Nyman, L. M. Eerola, S. Leppa, A high tumor-associated macrophage content predicts favorable outcome in follicular lymphoma patients treated with rituximab and cyclophosphamide-doxorubicin-vincristine-prednisone. *Clin Cancer Res* **13**, 5784-5789 (2007).
32. A. C. Drake, Q. Chen, J. Chen, Engineering humanized mice for improved hematopoietic reconstitution. *Cellular & molecular immunology* **9**, 215-224 (2012).
33. I. Leskov *et al.*, Rapid generation of human B-cell lymphomas via combined expression of Myc and Bcl2 and their use as a preclinical model for biological therapies. *Oncogene* **32**, 1066-1072 (2013).
34. T. J. Elliott, M. J. Glennie, H. M. McBride, G. T. Stevenson, Analysis of the interaction of antibodies with immunoglobulin idiotypes on neoplastic B lymphocytes: implications for immunotherapy. *J Immunol* **138**, 981-988 (1987).
35. A. L. Tutt *et al.*, Development and Characterization of Monoclonal Antibodies Specific for Mouse and Human Fcgamma Receptors. *J Immunol* **195**, 5503-5516 (2015).
36. B. Langmead, C. Trapnell, M. Pop, S. L. Salzberg, Ultrafast and memory-efficient alignment of short DNA sequences to the human genome. *Genome Biol* **10**, R25 (2009).
37. B. Li, C. N. Dewey, RSEM: accurate transcript quantification from RNA-Seq data with or without a reference genome. *BMC Bioinformatics* **12**, 323 (2011).
38. M. D. Robinson, D. J. McCarthy, G. K. Smyth, edgeR: a Bioconductor package for differential expression analysis of digital gene expression data. *Bioinformatics* **26**, 139-140 (2010).
39. D. W. Huang *et al.*, DAVID Bioinformatics Resources: expanded annotation database and novel algorithms to better extract biology from large gene lists. *Nucleic Acids Res* **35**, W169-175 (2007).

40. A. Subramanian *et al.*, Gene set enrichment analysis: a knowledge-based approach for interpreting genome-wide expression profiles. *Proc Natl Acad Sci U S A* **102**, 15545-15550 (2005).
41. F. O. Martinez, S. Gordon, M. Locati, A. Mantovani, Transcriptional profiling of the human monocyte-to-macrophage differentiation and polarization: new molecules and patterns of gene expression. *J Immunol* **177**, 7303-7311 (2006).
42. A. I. Saeed *et al.*, TM4: a free, open-source system for microarray data management and analysis. *Biotechniques* **34**, 374-378 (2003).
43. S. H. Lim *et al.*, Fc gamma receptor IIb on target B cells promotes rituximab internalization and reduces clinical efficacy. *Blood* **118**, 2530-2540 (2011).
44. A. C. Aschenbrenner, J. L. Schultze, New "programmers" in tissue macrophage activation. *Pflugers Archiv : European journal of physiology* **469**, 375-383 (2017).
45. J. Xue *et al.*, Transcriptome-based network analysis reveals a spectrum model of human macrophage activation. *Immunity* **40**, 274-288 (2014).
46. D. J. Slamon *et al.*, Use of chemotherapy plus a monoclonal antibody against HER2 for metastatic breast cancer that overexpresses HER2. *N Engl J Med* **344**, 783-792 (2001).
47. G. Chen *et al.*, A feasibility study of cyclophosphamide, trastuzumab, and an allogeneic GM-CSF-secreting breast tumor vaccine for HER2+ metastatic breast cancer. *Cancer Immunol Res* **2**, 949-961 (2014).
48. F. Arce Vargas *et al.*, Fc Effector Function Contributes to the Activity of Human Anti-CTLA-4 Antibodies. *Cancer Cell* **33**, 649-663 e644 (2018).
49. Y. Bulliard *et al.*, Activating Fc gamma receptors contribute to the antitumor activities of immunoregulatory receptor-targeting antibodies. *J Exp Med* **210**, 1685-1693 (2013).
50. M. R. York *et al.*, A macrophage marker, Siglec-1, is increased on circulating monocytes in patients with systemic sclerosis and induced by type I interferons and toll-like receptor agonists. *Arthritis Rheum* **56**, 1010-1020 (2007).
51. M. S. Macauley, P. R. Crocker, J. C. Paulson, Siglec-mediated regulation of immune cell function in disease. *Nat Rev Immunol* **14**, 653-666 (2014).
52. R. Wang, T. Town, V. Gokarn, R. A. Flavell, R. Y. Chandawarkar, HSP70 enhances macrophage phagocytosis by interaction with lipid raft-associated TLR-7 and upregulating p38 MAPK and PI3K pathways. *J Surg Res* **136**, 58-69 (2006).
53. A. Asea *et al.*, HSP70 stimulates cytokine production through a CD14-dependant pathway, demonstrating its dual role as a chaperone and cytokine. *Nature medicine* **6**, 435-442 (2000).
54. D. Petrovic-Djergovic *et al.*, CXCL10 induces the recruitment of monocyte-derived macrophages into kidney, which aggravate puromycin aminonucleoside nephrosis. *Clin Exp Immunol* **180**, 305-315 (2015).
55. Y. Zhan *et al.*, Ets-1 is a critical regulator of Ang II-mediated vascular inflammation and remodeling. *The Journal of clinical investigation* **115**, 2508-2516 (2005).
56. C. T. Rankin *et al.*, CD32B, the human inhibitory Fc-gamma receptor IIB, as a target for monoclonal antibody therapy of B-cell lymphoma. *Blood* **108**, 2384-2391 (2006).
57. A. Roghanian *et al.*, Antagonistic Human FcgammaRIIB (CD32B) Antibodies Have Anti-Tumor Activity and Overcome Resistance to Antibody Therapy In Vivo. *Cancer Cell* **27**, 473-488 (2015).
58. J. A. Burger, P. Ghia, A. Rosenwald, F. Caligaris-Cappio, The microenvironment in mature B-cell malignancies: a target for new treatment strategies. *Blood* **114**, 3367-3375 (2009).
59. R. Nahta, D. Yu, M. C. Hung, G. N. Hortobagyi, F. J. Esteva, Mechanisms of disease: understanding resistance to HER2-targeted therapy in human breast cancer. *Nat Clin Pract Oncol* **3**, 269-280 (2006).
60. L. A. Liotta, E. C. Kohn, The microenvironment of the tumour-host interface. *Nature* **411**, 375-379 (2001).

61. E. Bakker, M. Qattan, L. Mutti, C. Demonacos, M. Krstic-Demonacos, The role of microenvironment and immunity in drug response in leukemia. *Biochimica et biophysica acta* **1863**, 414-426 (2016).
62. M. B. Meads, L. A. Hazlehurst, W. S. Dalton, The bone marrow microenvironment as a tumor sanctuary and contributor to drug resistance. *Clin Cancer Res* **14**, 2519-2526 (2008).
63. A. N. Tikhonova *et al.*, The bone marrow microenvironment at single-cell resolution. *Nature*, (2019).

**Figure Legends**

**Figure 1. BM niche is resistant to mAb therapy and promotes immunosuppressive effector macrophages.** Ten million luciferase$^+$ GFP$^+$ CD20$^+$ human B cell lymphoma cells were intravenously injected into adult NSG mice and treated with either 10 mg/kg rituximab (Rit) or 100 mg/kg CTX as single agent or in combination on day 21 after tumor injection. Tumor burden as indicated by bioluminescence intensity was monitored on day 21 (before treatment) and 7 days after the indicted treatments. **(A)** Representative mouse images and **(B)** bioluminescence signal intensity in the BM. The positions of the spleen and BM are indicated. Each dot represents one mouse.; * $p$ <0.05, **** $p$ <0.0001 by one-way ANOVA test. **(C)** Representative flow cytometry histograms of FcγR expression on F4/80$^+$ macrophages from spleen and BM of a plain NSG mouse (n = 5). Red trace: isotype control (iso); orange trace: spleen; blue trace: BM, as indicated. **(D)** CD68$^+$ macrophages express higher levels of FcγRIIB in the BM than in the lymph node in lymphoma patients. FFPE diagnostic LN biopsies and staging BM trephines from three consented patients with follicular lymphoma were double-stained with antibodies to human CD68 (pink) and FcγRIIB (brown). Paired LN and BM samples from each patient were mounted on the same slide and stained. Representative IHC images are shown (original magnification x400; scale bar is 20μm) from areas with high lymphoma burden (left panel) and areas with no lymphoma involvement (right panel). The insert in each image represents 10x higher magnification of a representative macrophage taken from the same section. Black arrows point to CD68$^+$ macrophages in the LN and BM.

**Figure 2. CTX treatment induces a higher A:I FcγR ratio in BM-resident, but not splenic, macrophages in non-tumor-bearing mice. (A)** FcγR expression on F4/80$^+$ macrophages in the BM 1, 2 and 3 days after CTX treatment normalized to corresponding FcγR expression on untreated F4/80$^+$ macrophages in the BM of control non-treated (NT) mice. Mean ±SD shown; n = 5 mice/group. **(B-D)** Comparison of FcγR expression by F4/80$^+$ macrophages in the BM and spleen of NT and CTX-treated NSG mice (2 days). (**B**) Representative flow cytometry histograms of various

FcγR expression by BM F4/80$^+$ macrophages. Red trace: isotype control; blue trace: NT; orange trace: CTX treatment. Comparison of FcγR expression by F4/80$^+$ macrophages in the (**C**) BM and (**D**) spleen of NT and CTX-treated NSG mice (2 days after CTX treatment). (**E-F**) Comparison of A:I FcγR ratio on F4/80$^+$ macrophages from **(E)** BM and **(F)** spleen of NT and CTX-treated mice. **(G)** Representative flow cytometry histograms showing MHC class II and CD86 expressing by BM F4/80$^+$ macrophages. Red trace: isotype control; blue trace: NT; orange trace: CTX-treated (day 2). Each dot in C-F represents one mouse; ** $p < 0.001$, *** $p < 0.0001$ by Mann-Whitney test.

**Figure 3. CTX treatment enhances A:I FcγR ratio in lymphoma-bearing mouse BM macrophages. (A)** Comparison of FcγR expression on BM F4/80$^+$ macrophages from non-tumor-bearing (filled symbols) and lymphoma-bearing (open symbols; shaded boxes) NSG mice. FcγR expression was assayed 21 days following intravenous injection of 1x10$^7$ lymphoma cells. **(B)** Representative flow cytometry histograms of the inhibitory FcγRIIB expression on BM F4/80$^+$ macrophages. Red trace: isotype control; orange trace: non-tumor-bearing mouse; blue trace: tumor-bearing mouse. **(C-D)** Comparison of median fluorescence intensity of activatory and inhibitory FcγRs on F4/80$^+$ macrophages from the **(C)** BM and **(D)** spleen of lymphoma-bearing mice with or without CTX treatment. **(E-F)** Comparison of A:I FcγR ratio on F4/80$^+$ macrophages from the **(E)** BM and **(F)** spleen of tumor-bearing mice with or without CTX treatment (day 2). Each dot represents one mouse; * $p$ <0.05, ** $p$ <0.001 by Mann-Whitney test.

**Figure 4. BM-resident human B cells are resistant to rituximab-mediated depletion, but are sensitized by CTX treatment.** Adult humanized mice were injected with 10 mg/kg rituximab (Rit). Mice were bled on day 2, 5 and 7 and the percentage of human (h) CD19$^+$ B cells was quantified (n = 3 mice/group). **(A)** Shown are percentages of human CD19$^+$ B cells normalized to the percentage of B cells in the same mouse prior to rituximab treatment; *** $p$ <0.001 by one-way ANOVA test. **(B)** Seven days after rituximab treatment, single cell suspensions were prepared from harvested organs

and assayed for human $CD45^+$ $CD19^+$ B cells by flow cytometry. Shown are hCD19 versus hCD3 staining profiles from the blood, spleen and the BM of a representative mouse. The numbers indicate percentages of cells in the respective gate. **(C-D)** Humanized mice were intraperitoneally injected with either 10 mg/kg Rit or 100 mg/kg CTX as single agent or in combination. **(C)** Organs were harvested 7 days post treatment and percentage of live $hCD45^+hCD19^+$ B cells were quantified in the BM and spleen. Each dot represents one mouse; *$p$ <0.05, **$p$ <0.001 by one-way ANOVA test. **(D)** Representative flow cytometry plots showing hCD19 versus hCD3 staining profiles from spleen and the BM of representative mice.

**Figure 5. CTX potentiates mAb-mediated depletion of human breast cancer cells in the BM.** Adult NSG **(A-E)** or humanized mice **(F-G)** were engrafted with $5x10^4$ MDA-MB-231 breast cancer cells by intracardiac injection. Randomized tumor-bearing mice and treated with either 10 mg/kg of the indicted therapeutic mAb or 100 mg/kg CTX as single agent or in combination on day 10, 15 and 20 post tumor engraftment. Bioluminescence intensities were assessed by IVIS imaging on the indicated days. **(A)** Representative mouse images and **(B)** quantifications of bioluminescence intensity shown. **(D)** Representative H&E stains of femur sections (40x) of mice at day 20 after tumor engraftment. Inserts: tibia and femur from representative mice. **(D)** Bone lesions were scanned by micro CT at the indicated days; sizes of lesions (mean ±SD) are shown overtime. **(E)** Survival of cohorts of mice with different treatments. Trastuzumab and cetuximab alone or plus CTX were used, as indicated. **(F)** Representative bioluminescent images and **(G)** quantifications of tumor-bearing humanized mice. 3-5 mice/group, repeated at least 3 times for each experiment; ** $p$ <0.001, ** $p$ <0.001 by Mann-Whitney test.

**Figure 6. Transcriptome analysis of human and mouse macrophages from spleen and BM of CTX-treated humanized mice.** Adult humanized mice were injected with 100 mg/kg CTX and 2 days later spleen and BM were harvested. Both mouse and human macrophages were purified by cell

sorting and subjected to RNAseq analysis (m: mouse; h: human). **(A)** PCA analysis of spleen (Sp) and BM $CD45^{+}CD14^{+}$ human and $F4/80^{+}$ mouse macrophages. **(B)** Heatmap showing differentially expressed genes specifically induced by CTX in the mouse macrophages in the spleen or BM or both tissues, along with gene fold-changes in each organ following CTX treatment. **(C)** Functional pathway enrichment analysis of differentially expressed genes induced by CTX in the mouse macrophages. **(D)** GSEA analysis showing positive coloration with mouse TNF-α (NES = 1.89; FWER $p$ = 0.003) and IFN-γ (NES = 1.95; FWER $p$ < 0.001) signaling elements. **(E)** Heatmap representation of FcγR genes in spleen and BM of mouse macrophages, along with their respective fold changes following CTX treatment; and a graph showing calculated A:I FcγR ratios for macrophages isolated from each organ pre- and post-treatment (*$p$ <0.05). **(F)** Heatmap showing differentially expressed genes specifically induced by CTX in the human macrophages in the spleen or BM or both tissues, along with gene fold-changes in each organ following CTX treatment. **(G)** Functional pathway enrichment analysis of differentially expressed genes induced by CTX in the human macrophages in the spleen and BM. **(H)** GSEA analysis showing positive coloration with human TNF-α (NES = 1.86; FWER $p$ <0.001) and IFN-γ (NES = 3.01; FWER $p$ <0.001) signaling elements. **(I)** Heatmap showing differentially expressed genes induced by CTX in both mouse and human macrophages in the spleen and the BM, respectively. NES; normalized enrichment score; FWER; familywise-error rate.

Figure 1.

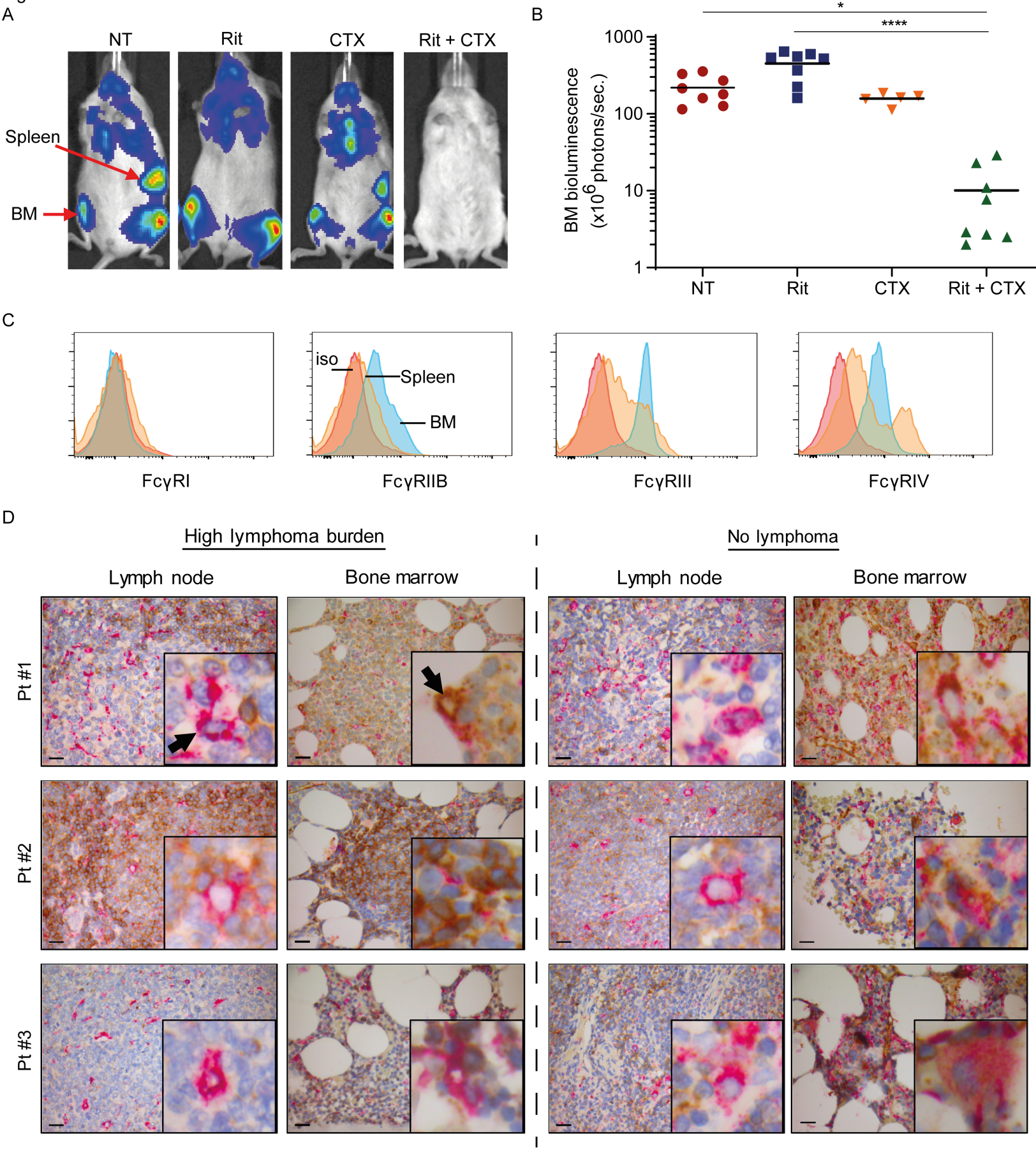
A
NT
Rit
CTX
Rit + CTX
Spleen
BM
B
*
****
1000
100
10
1
BM bioluminescence (x10^6 photons/sec.)
NT
Rit
CTX
Rit + CTX
C
iso
Spleen
BM
FcγRI
FcγRIIB
FcγRIII
FcγRIV
D
High lymphoma burden
No lymphoma
Lymph node
Bone marrow
Lymph node
Bone marrow
Pt #1
Pt #2
Pt #3

Figure 2.

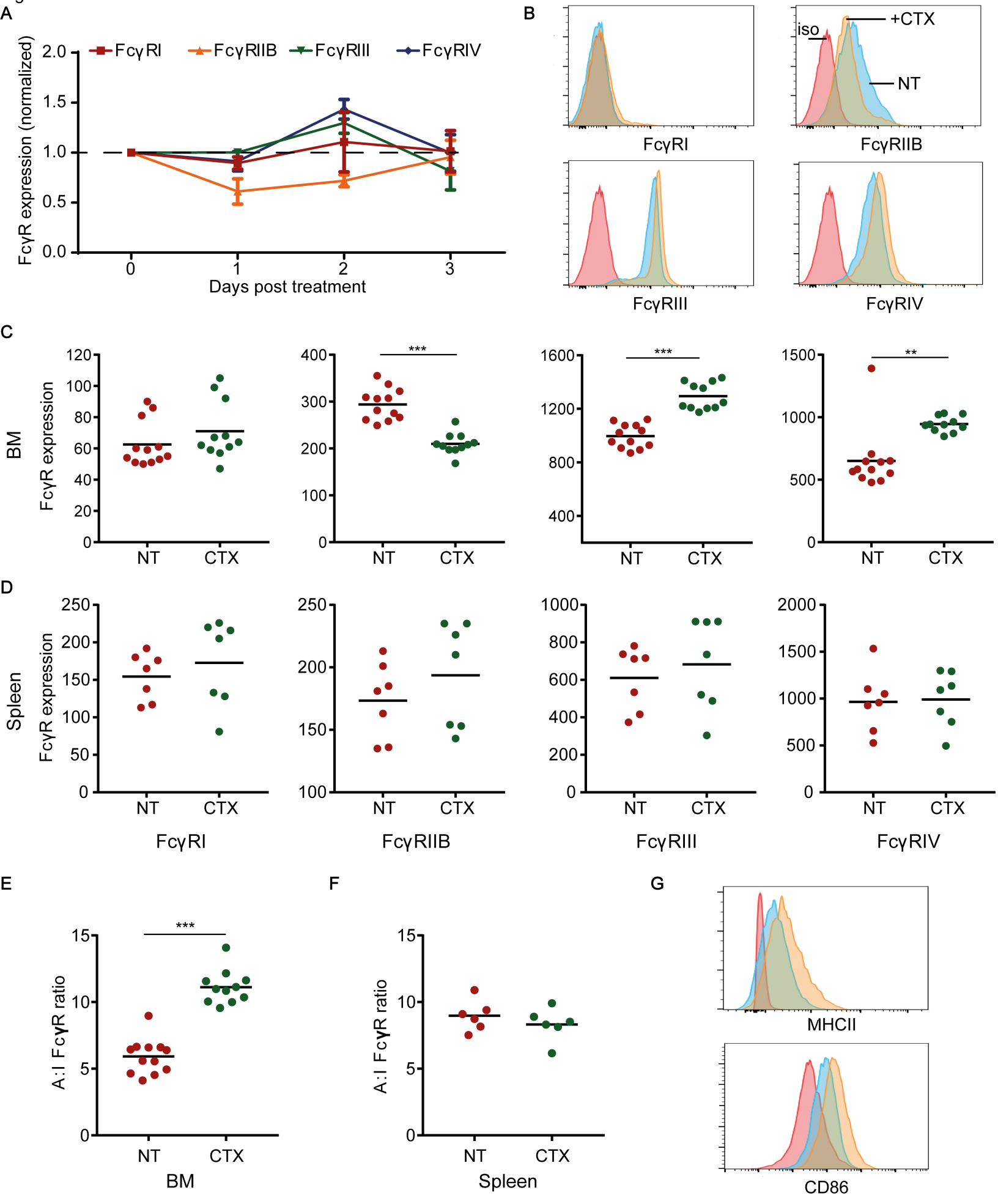
A
FcγR expression (normalized)
FcγRI
FcγRIIB
FcγRIII
FcγRIV
Days post treatment
B
iso
+CTX
NT
FcγRI
FcγRIIB
FcγRIII
FcγRIV
C
BM
FcγR expression
NT
CTX
***
**
D
Spleen
FcγR expression
FcγRI
FcγRIIB
FcγRIII
FcγRIV
E
A:I FcγR ratio
BM
F
A:I FcγR ratio
Spleen
G
MHCII
CD86

Figure 3.

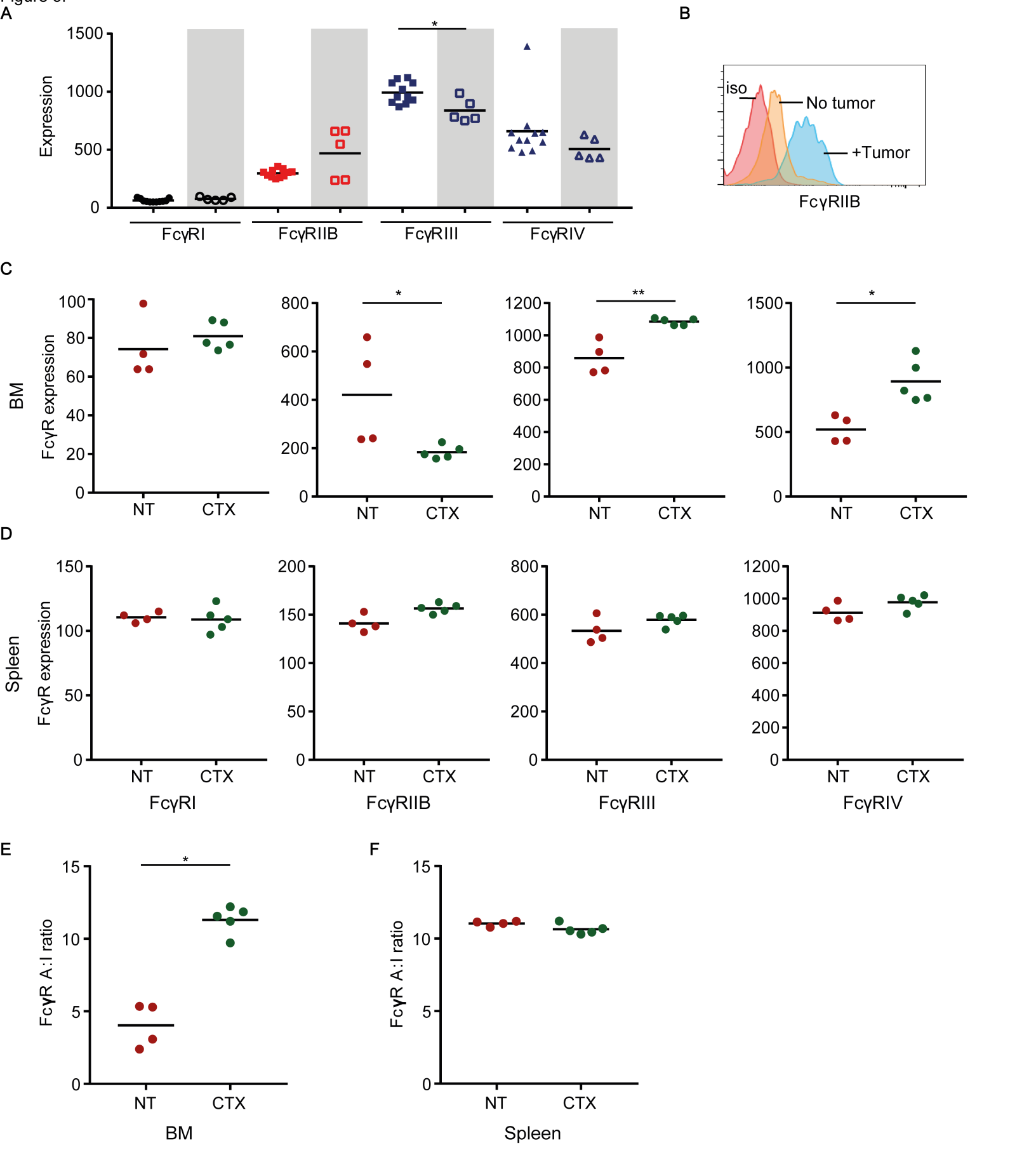
A
Expression
1500
1000
500
0
*
FcγRI
FcγRIIB
FcγRIII
FcγRIV
B
iso
No tumor
+Tumor
FcγRIIB
C
BM
FcγR expression
NT
CTX
*
**
*
D
Spleen
FcγR expression
FcγRI
FcγRIIB
FcγRIII
FcγRIV
E
FcγR A:I ratio
BM
F
FcγR A:I ratio
Spleen

Figure 4.

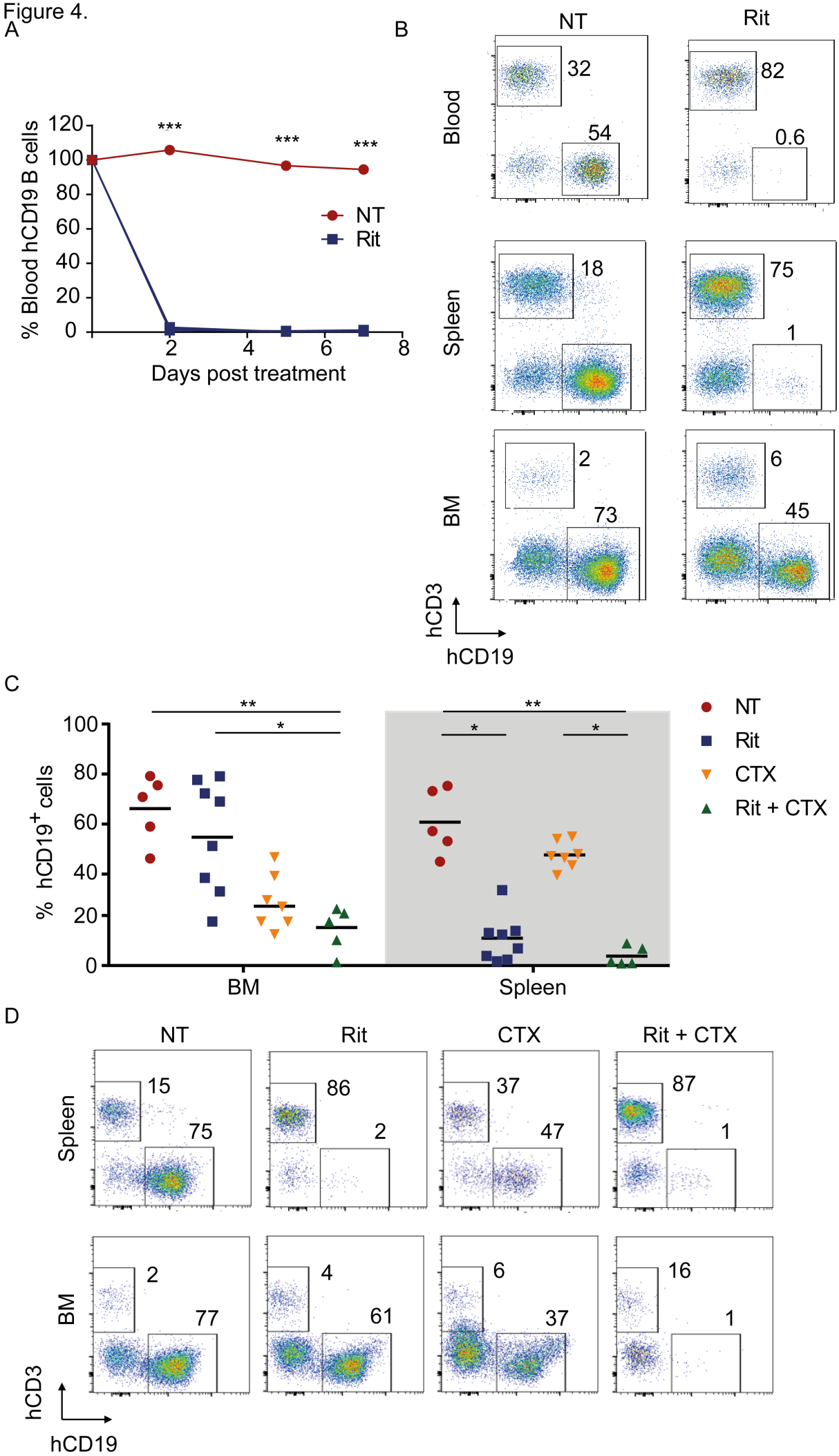
A
% Blood hCD19 B cells
120
100
80
60
40
20
0
***
***
***
NT
Rit
2
4
6
8
Days post treatment
B
NT
Rit
Blood
32
54
82
0.6
Spleen
18
1
75
1
BM
2
73
6
45
hCD3
hCD19
C
% hCD19+ cells
100
80
60
40
20
0
**
*
**
*
*
BM
Spleen
NT
Rit
CTX
Rit + CTX
D
NT
Rit
CTX
Rit + CTX
Spleen
15
75
86
2
37
47
87
1
BM
2
77
4
61
6
37
16
1
hCD3
hCD19

Figure 5.

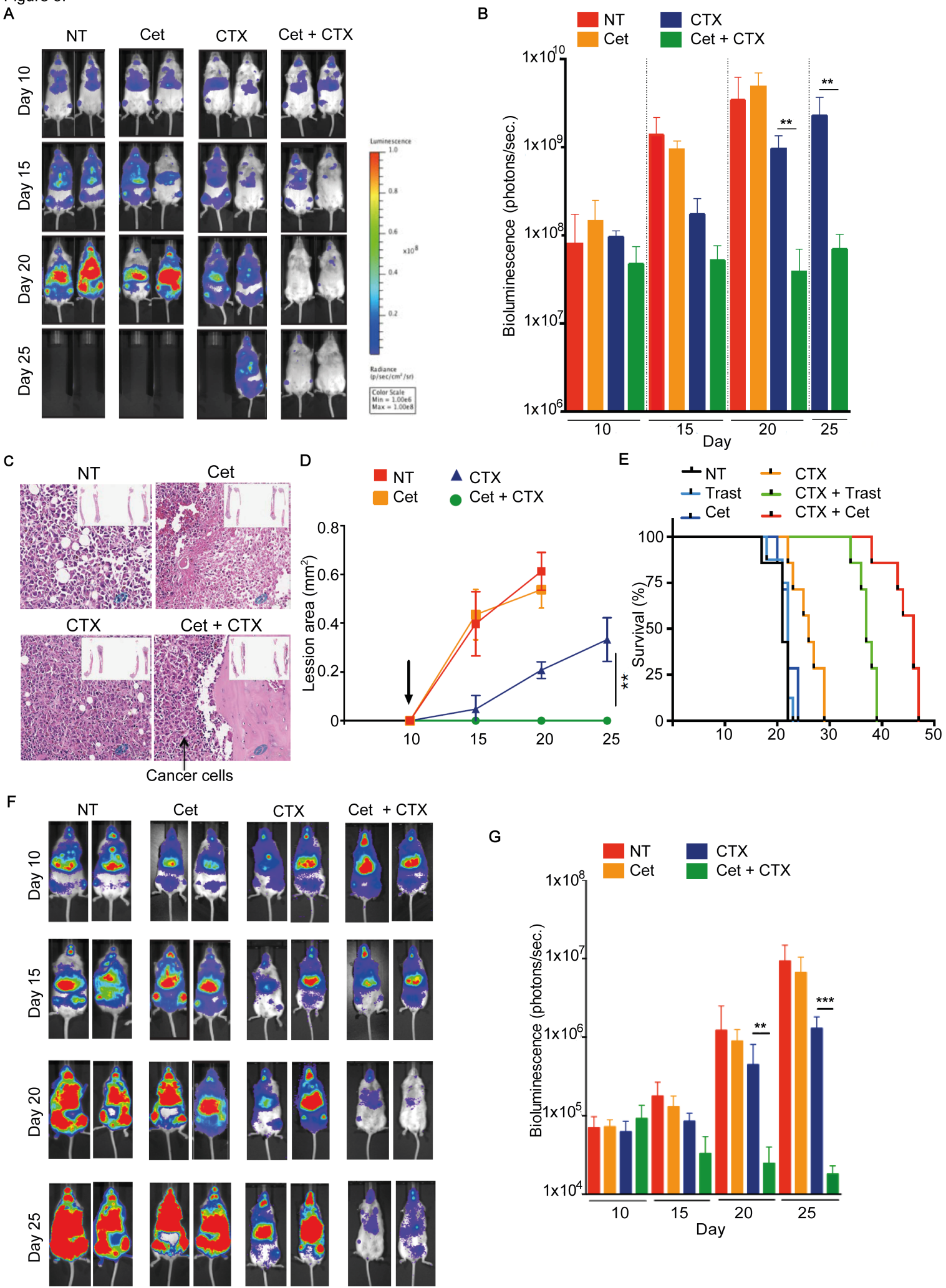
A
NT
Cet
CTX
Cet + CTX
Day 10
Day 15
Day 20
Day 25
Luminescence
Radiance (p/sec/cm²/sr)
Color Scale Min = 1.00e6 Max = 1.00e8
B
NT
Cet
CTX
Cet + CTX
Bioluminescence (photons/sec.)
Day
**
C
NT
Cet
CTX
Cet + CTX
Cancer cells
D
NT
Cet
CTX
Cet + CTX
Lession area (mm²)
**
E
NT
Trast
Cet
CTX
CTX + Trast
CTX + Cet
Survival (%)
F
NT
Cet
CTX
Cet + CTX
Day 10
Day 15
Day 20
Day 25
G
NT
Cet
CTX
Cet + CTX
Bioluminescence (photons/sec.)
Day
**
***

Figure 6.

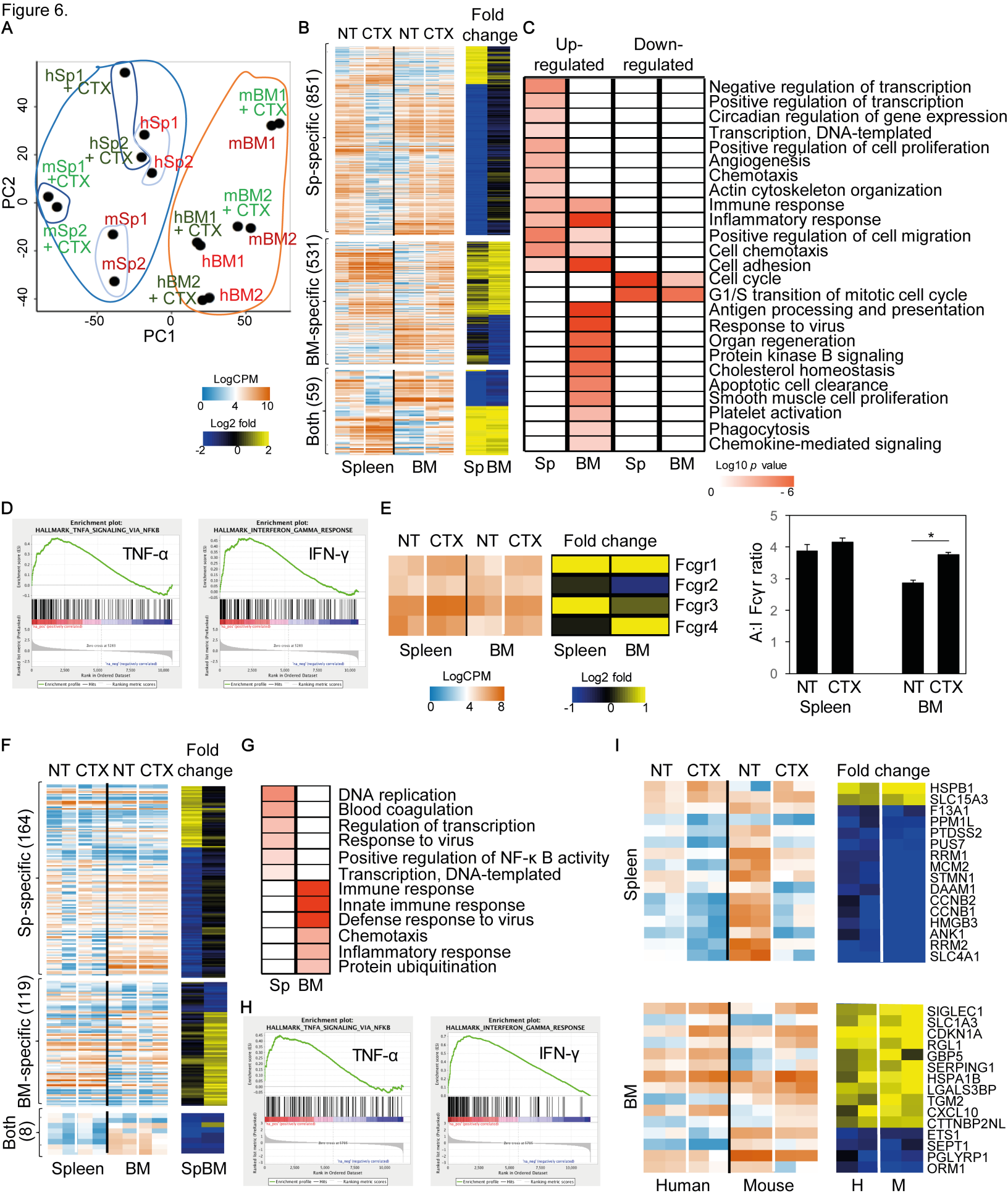
A
hSp1 + CTX
hSp1
hSp2 + CTX
hSp2
mSp1 +CTX
mSp1
mSp2 + CTX
mSp2
mBM1 + CTX
mBM1
mBM2 + CTX
mBM2
hBM1 + CTX
hBM1
hBM2 + CTX
hBM2
PC1
PC2
LogCPM
Log2 fold
B
NT CTX NT CTX
Fold change
Sp-specific (851)
BM-specific (531)
Both (59)
Spleen BM
Sp BM
C
Up-regulated
Down-regulated
Negative regulation of transcription
Positive regulation of transcription
Circadian regulation of gene expression
Transcription, DNA-templated
Positive regulation of cell proliferation
Angiogenesis
Chemotaxis
Actin cytoskeleton organization
Immune response
Inflammatory response
Positive regulation of cell migration
Cell chemotaxis
Cell adhesion
Cell cycle
G1/S transition of mitotic cell cycle
Antigen processing and presentation
Response to virus
Organ regeneration
Protein kinase B signaling
Cholesterol homeostasis
Apoptotic cell clearance
Smooth muscle cell proliferation
Platelet activation
Phagocytosis
Chemokine-mediated signaling
Sp BM Sp BM
Log10 p value
D
Enrichment plot: HALLMARK_TNFA_SIGNALING_VIA_NFKB
TNF-α
Enrichment plot: HALLMARK_INTERFERON_GAMMA_RESPONSE
IFN-γ
E
NT CTX NT CTX
Fold change
Fcgr1
Fcgr2
Fcgr3
Fcgr4
Spleen BM
Spleen BM
LogCPM
Log2 fold
A:I Fcyr ratio
*
NT CTX NT CTX
Spleen BM
F
NT CTX NT CTX
Fold change
Sp-specific (164)
BM-specific (119)
Both (8)
Spleen BM SpBM
G
DNA replication
Blood coagulation
Regulation of transcription
Response to virus
Positive regulation of NF-κ B activity
Transcription, DNA-templated
Immune response
Innate immune response
Defense response to virus
Chemotaxis
Inflammatory response
Protein ubiquitination
Sp BM
H
Enrichment plot: HALLMARK_TNFA_SIGNALING_VIA_NFKB
TNF-α
Enrichment plot: HALLMARK_INTERFERON_GAMMA_RESPONSE
IFN-γ
I
NT CTX NT CTX
Fold change
Spleen
HSPB1
SLC15A3
F13A1
PPM1L
PTDSS2
PUS7
RRM1
MCM2
STMN1
DAAM1
CCNB2
CCNB1
HMGB3
ANK1
RRM2
SLC4A1
BM
SIGLEC1
SLC1A3
CDKN1A
RGL1
GBP5
SERPING1
HSPA1B
LGALS3BP
TGM2
CXCL10
CTTNBP2NL
ETS1
SEPT1
PGLYRP1
ORM1
Human Mouse
H M